Original papers

Med Ultrason 2019, Vol. 21, no. 4, 389-398
DOI: 10.11152/mu-2006

Stitching of 3D ultrasound datasets for the determination of large thyroid volumes – phantom study part II: mechanically-swept probes

Philipp Seifert, Thomas Winkens, Leonard Knichel, Christian Kühnel, Martin Freesmeyer

Clinic of Nuclear Medicine, Jena University Hospital, Jena, Germany

Abstract

Aims: To investigate the feasibility and accuracy of 3D-US extended field of view volumetric analyses acquired with mechanically-swept ultrasound probes with different measurement methods for large volume thyroid phantoms. **Materials and methods**: Fifteen thyroid phantoms with different shapes (regular, nodular, thickened isthmus) and volumes (50-400 mL) were created. Two different mechanically-swept US probes were used for the separate scanning of the left and right lobes: convex and linear probe. After specific modifications, the 3D-US datasets were stitched together to an extended field of view using predefined landmarks. Volumetric analyses were performed by conventional ellipsoid model and manual tracing methods. The correspondence of measured and reference volumes was calculated using Pearson's correlation coefficients and limits of agreement according to Bland and Altman. **Results**: The C-probe proved feasible for the acquisition and processing of the three-dimensional ultrasound extended field of view images; very high levels of agreement (correlation coefficients for volume analyses: 0.9843-0.9992) were observed for all shapes and volumes investigated. The manual tracing method showed superior results in comparison to the ellipsoid model, but was more time consuming. The linear probe was only applicable for the 50 mL phantoms due to its limited field of view. **Conclusions**: The investigated mechanically-swept convex probe was suitable for the three-dimensional ultrasound extended field of view stitching of large volume thyroid phantoms. Accurate volume analyses could be carried out. The mechanically-swept linear probe is limited to a maximum of 50 mL.

Keywords: 3D-US; thyroid phantoms; extended field of view; ellipsoid model; mechanically-swept probes

Introduction

Over 10% of the world population have an enlarged thyroid gland with or without nodules. The main causes are environmental factors, in particular regional iodine intake, as well as individual factors such as gender, age, genes, and consumption behavior. However, size and shape of the thyroid glands are subject to a wide variability and large multinodular goiters continue to appear relatively frequently in clinical practice [1-5].

Ultrasonography (US) remains the basic diagnostic tool for thyroid imaging [6,7]. Accurate volume measurements are particularly important for activity calculations in preparation of radioiodine therapy and the assessment of its effectiveness [8,9]. High anatomical resolution with favorable soft-tissue contrast, absence of contraindications or radiation exposure, cost-effectiveness, and ubiquitous availability are well-known benefits of US in comparison to competing methods such as magnetic resonance imaging (MRI) and computed tomography (CT) [10].

Today's clinical standard comprises two-dimensional US imaging (2D-US) of the thyroid gland [11]. Assum-

Received 29.04.2019 Accepted 15.07.2019
Med Ultrason
2019, Vol. 21, No 4, 389-398
Corresponding author: PD Dr. med. Martin Freesmeyer, M.D.
Clinic of Nuclear Medicine
Jena University Hospital
Am Klinikum 1, 07747 Jena, Germany
Phone: +49-3641-9329801
Fax: +49-3641-9329802
E-mail: martin.freesmeyer@med.uni-jena.de

ing that the thyroid lobes have an ideal shape, which is reasonably appropriate for ordinary thyroid glands, the ellipsoid model (em) is universally applied for volumetric analyses [12]. However, anatomical variants and diseases cause significant changes of the organs morphology and thereby can affect the accuracy of measurements. Furthermore, inter- and intra-observer variability may lead to remarkable volumetric errors, especially in case of large volume thyroid glands with several shape deformations [12-15].

The use of three-dimensional ultrasound (3D-US) enables the operator to generate volume datasets in three dimensions, store them to Picture Archiving and Communication Systems (PACS), and perform post hoc volumetric analyses [16,17]. In addition, 3D-US allows the use of contour-based slice-wise manual tracing (mt) analogues to sectional imaging in MRI and CT [18]. It has been shown that this method reaches very high levels of agreement with the actual thyroid volumes [19]. However, heavily enlarged thyroid glands may exceed the field of view (FOV) of common 3D probes, inhibiting comprehensive recording of the whole organ with one single scan [17,20]. Several approaches have been introduced to overcome this limitation, e.g. by creating extended FOV (EFOV) 3D-US images using optical tracking of a calibrated 3D-US probe which has a 2D transducer array [21]. Another possible solution to overcome the spatial limitations, the post hoc assembly of two or more 3D-US datasets by means of the stitching method, has been recently published [22]. Stitching allows the generation of a jointed volume dataset out of several single US scans, leading to an EFOV. The introduced phantom study, using sensor-navigated (sn) US probes, confirmed the feasibility of the method even in large thyroid phantoms (up to 400 mL) [22].

However, sn 3D-US is a magnet-based technology and therefore requires specific equipment: an externally installed magnet (creating the magnetic field) and magnetic sensor-clips attached to the US probes (tracking the spatial orientation of the probe within the magnetic field). Magnetic fields are interference-prone and the sensor-clips can impede the accessibility of human thyroid glands in sagittal orientation, especially in the case of obesity or narrow cervical anatomy. In addition, sn US probes are rarely used in clinical practice, whereas mechanically-swept (ms) approaches are more widely established, especially in gynecology [23].

Therefore, the first purpose of the current study is to investigate whether stitching of two separately acquired 3D-US datasets of large volume thyroid phantoms (with several volume and shape variants) is feasible with ms US probes, too. The previous sn 3D-US study showed very high correlation coefficients between the measured and the reference volumes, revealing superior data for the mt method in comparison to the em approach [22]. Thus, the second aim of this study is to investigate whether similar results for volumetric analyses can be achieved with ms US probes.

Materials and methods

Phantoms

Fifteen water-filled, heart-shaped balloons were created based on previously introduced methods [12,22]. The phantoms were produced with several shape variations in 15 predefined volumes (50, 75, 100, 125, 150, 175, 200, 225, 250, 275, 300, 325, 350, 375, and 400 mL) (fig 1). To reproduce the lobes of a normal thyroid gland, a median clamp was applied simulating the typically narrow isthmus (fig 1a and 1b).

For US imaging, the phantoms were placed 2 cm below the water surface of a double-walled, water-filled plastic container. Four tiny plastic pieces were inserted into the balloons and then ligated to the wall of the inner plastic container with two threads per pole (fig 2). Besides the isthmus clamp, three landmarks per side were fixed onto the front of the phantom. The landmarks, consisting of echogenic hybrid polymer glue (Fix All Classic, Soudal, Leverkusen, Germany) served as orientation points for post hoc stitching of the separately acquired 3D-US datasets. A 2 cm diameter polymethylmethacrylate (Perspex®, Billingham, UK) rod fixed onto styrofoam 2 cm above the bottom simulated the human trachea. The phantoms were stretched along the rod and fixed with threads as previously described to simulate an anthropomorphic shape of the thyroid gland (fig 2a).

The tare weight of each empty balloon was measured using a precision scale. Subsequently, pre-boiled water (to minimize air bubbles) was filled into the balloons. The net volumes, representing the reference standard for volumetric accuracy assessment were achieved by weight measurements. A second weight measurement was carried out after the experiments to exclude leakages.

The 3D-US images were acquired in three cycles: first, with normal-shaped thyroid phantoms (fig 1a), secondly with lobe deformations achieved by ligations to simulate nodular goiters (fig 1b), and third, by removing the isthmus clamp to simulate a thickened isthmus (fig 2c).

Ultrasonography scans

All scans were performed with the Logiq E9 US device (General Electric Medical Systems, Milwaukee, WI, USA). In contrast to the previously published data based on the use of sn US probes [22], ms US probes

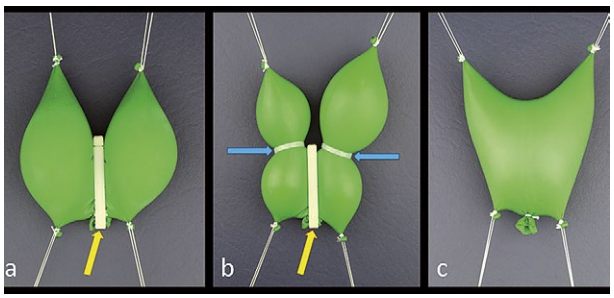

Fig 1. Shape variants of the thyroid phantoms (volumes: 50 mL each): Regular shape with isthmus simulation by means of a median clamp (yellow arrow) (a), nodular shape with lobe bindings (blue arrows) (b), and thickened isthmus shape without clamp or bindings (c).

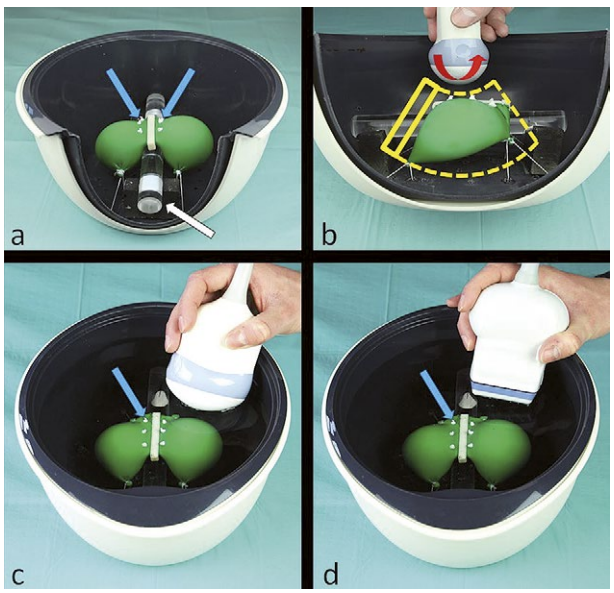

Fig 2. 3D-US set-up: Phantom sample (volume: 200 mL) with hybrid polymer landmarks (blue arrows) used for stitching guidance (a). A Perspex® rod (white arrow) serves as trachea imitation and construction aid. An array inside the convex RAB4-8 probes (C-probe) housing automatically moves in craniocaudal direction (red arrow) (b). The yellow box represents the field-of-view (FOV) of the mechanically-swept (ms) probes. US scanning in a water-filled container via C-probe (c) and a linear RSP6-16 probe (L-probe) (d).

were applied in the present study. Two different volume probes with incorporated motorized arrays, specifically the convex RAB4-8 probe (C-probe) (fig 2b, 2c, 3a, and 3b) and the linear RSP6-16 probe (L-probe) (fig 2d), were utilized. The automatically swept arrays enabled a dedicated area to be scanned without moving the probes housing (fig 2b), creating 3D volume datasets. Separate scans of the phantoms' right and left lobes were carried out. The probes were held fixed and the image acquisitions were performed in axial orientation. The inclusion

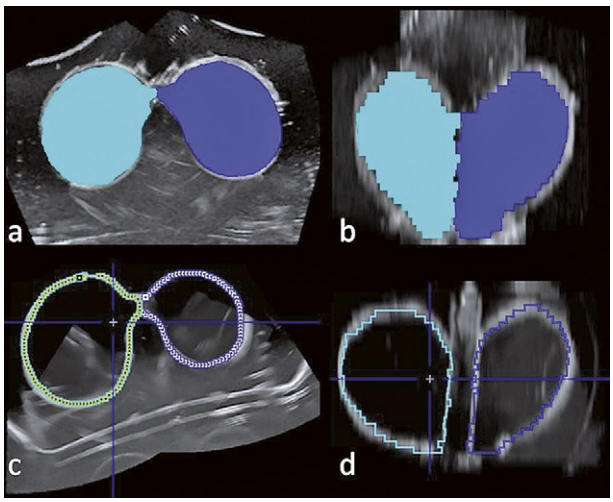

Fig 3. Manual tracing (mt) volumetric analyses of 3D-US extended field of view (EFOV) images of a 200-mL phantom sample acquired with the convex RAB4-8 probe (C-probe). Slice-wise manually contouring for volume data generation, depicted in transverse (a, c) and coronal (b, d) orientation (right lobe: turquoises, left lobe: blue) for clinical software (a, b) and research software (c, d).

of the isthmus ensured that each scan comprised the three ipsilateral and three contralateral landmarks (fig 3).

The US parameters were optimized to the following device specific presets: *C-probe*: transmitting power: 80%, number of foci: 1 (depth was manually optimized), contrast harmonic imaging: on, dynamic range: 51 dB, cross beam: maximum, volume angle: maximum (84°), b-mode quality: maximum, speckle reduction imaging (SRI): 4, grey scale: D; *L-probe*: transmitting power: 22%, number of foci: 1(depth was manually optimized), contrast harmonic imaging: on, dynamic range: 36 dB, cross beam: maximum, volume angle: maximum (84°), b-mode quality: Hi2 (maximum), speckle reduction imaging (SRI): 4, grey scale: J.

Digital Imaging and Communications in Medicine (DICOM) export and pre-stitching data modification

Local storage of the 3D-US volume datasets was performed using a specific DICOM standard for 3D-US (Enhanced Ultrasound Volume Storage; EUVS). Subsequently, the data were transferred to an external storage medium. In contrast to the sn approach [22], the current ms datasets required modifications of size specifications. After transferring the data from the US device to the computer software PMOD (software version 3.409, PMOD Technologies Ltd., Zurich, Switzerland), we noticed that the edge lengths of the image voxels were incorrect and did not fit in an appropriate rectangular matrix. This manufacturer-specific bug was probably caused

by voxel deformations due to the diversified US beam which particularly affects the distant reflections. The pixel edge length was digitally calibrated to the fixed size of the penetration depth with PMOD, and thus a correct indication of the voxel edge length could be restored.

Stitching and post-stitching data modification

Subsequently, the respective 3D-US scans of the left and right lobes were transferred to the stitching module of PMOD. The semi-transparently displayed images were aligned until the six landmarks were superimposed in axial and sagittal orientation (fig 3e). The newly created extended 3D-US datasets then included both lobes of the phantom and were locally stored (fig 3e). To reduce the time expenditure for mt volumetric analyses, the extended 3D-US datasets were converted to a uniform slice thickness of 3.0 mm using PMOD software as previously described [12].

In contrast to the sn data [22], the bit depth of the pixels and the DICOM format had to be adapted for cs usage, because cs only accepts manufacturer-specific CT data sets for volumetric analyses. This modification was carried out with the software Sante DICOM Editor (Version 5.0.2., Santesoft Ltd., Athens, Greece).

Volumetric analyses

One experienced investigator performed all volumetric analyses. The datasets were assessed by means of both the em ($length_{max}$ x $width_{max}$ x $depth_{max}$ x 0.5) and the mt method. In contrast to the previously reported sn-based study [22], mt was performed using two different software tools: "CT-Tool" of syngo Multimodality Workplace (Version VE40A, Siemens AG, Munich, Germany) = clinical software (cs) and "image viewing and volume of interest analysis" tool of PMOD = research software (rs).

The em measurements were carried out separately for each lobe starting with the maximum cranial-caudal diameter (length) in sagittal orientation. Subsequently, the maximum medial-lateral (width) and anterior-posterior (depth) diameters were measured in transverse orientation. In the case of phantoms with thickened isthmus, the isthmus volume was divided and assigned to the volumes of the respective right or left lobe; no separate isthmus measurement was carried out.

The mt method was manually performed by the operator, drawing individual regions of interest (ROI) according to the phantoms' contours in parallel transversal slices (fig 4a) with cs (fig 4a, b) and rs (fig 4c, d), respectively. Analogous to the em method, left and right lobes were assessed separately. Exceptions were the phantoms with thickened isthmus, in which a single holistic contour was drawn covering the right lobe, the left lobe, and the isthmus. Volume calculations were automatically output by the software.

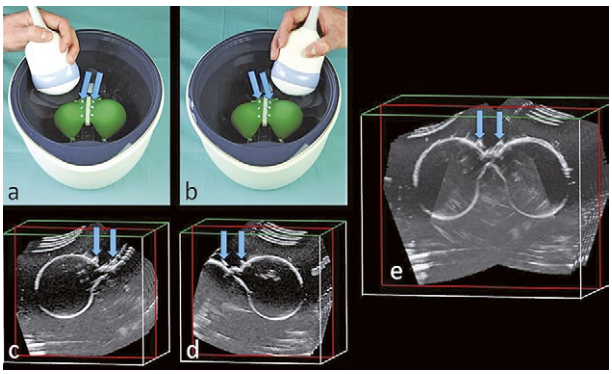

Fig 4. 3D-US of each lobe (a, b) and partial volume stitching (c-e): Sequential data acquisition of the left (a) and right lobe (b) of a 200-mL phantom sample using the convex RAB4-8 probe (C-probe). The two 3D-US datasets (c, d) were stitched together (e) in PMOD software using the apposite bilateral landmarks (blue arrows).

Statistical analysis

The relationships between the measured and reference volumes of the thyroid phantoms was calculated using Pearson's correlation coefficient. The deviation of measured volumes were calculated as percentage of the reference volumes by means of a slightly modified version of the Bland and Altman method [24]. These relative differences were described by mean, standard deviation (SD), median, range (minimum, maximum), and the 95% confidence intervals (CI) of the mean [25]. If the confidence interval did not include a zero value, the corresponding method had a significant systematic error (significance level 0.05, overestimation or underestimation of the reference volume). Additionally, measured and reference volumes were compared using the limits of agreement (mean + 1.96*SD) [24]. Assuming normal distribution, these intervals included 95% of all differences. The statistical calculations were performed using the Stata/IC software for Windows (software version 13.1, StataCorp LP, College Station, TX, USA).

Results

The C-probe was suitable to investigate differently sized and shaped large volume thyroid phantoms (50-400 mL). All phantoms could be satisfactorily examined according to the intent of the study with the C-probe. However, the L-probe was only applicable to the 50 mL phantoms. The assessable scanning area (FOV) was limited by the structural design of the probe due to its linear array construction. The angle of the incorporated motorized ms array was not wide enough to capture the full extent of large volume phantoms, especially the cranial-caudal diameter (length). Furthermore, in contrast to other linear

probes (such as the previously investigated sn probes), the virtual convex mode was not available for the L-probe when using the 3D mode, resulting in a bilateral restriction of the FOV. Therefore, L-probe volume analyses could only be carried out for the 50 mL phantoms.

Nevertheless, stitching of the obtained datasets via PMOD proved feasible for both probes. Fully captured phantoms in 3D-US EFOV were successfully subjected to volumetric analyses with both the em and mt methods.

Acquisition of a complete ms 3D-US dataset (right and left lobe) took 2-3 minutes regardless of the selected US probe. The pre-stitching modification of the voxel edge length for the ms datasets lasted about 2-3 minutes. For the stitching of two corresponding scans an average time expenditure of 4 minutes was necessary. Adjusting the bit depth and DICOM format for the cs took about 10 minutes per dataset. The duration of mt measurements were 15-20 minutes, while the em measurements took 1-2 min (fig 5).

The correlation coefficients between the measured and reference volumes (in respect to the measurement results of all phantom sizes), the mean values, medians, SDs, ranges, 95% CI, and limits of agreement for all three phantom shapes (regular, nodular, thickened isthmus), both volumetric analyses methods (em and mt), and both software types (cs and rs), are presented in Table I. The high correlation coefficients (0.9843-0.9992), irrespective of the measurement method or phantom shape, indicate a very strong positive relationship between the measured and reference volumes.

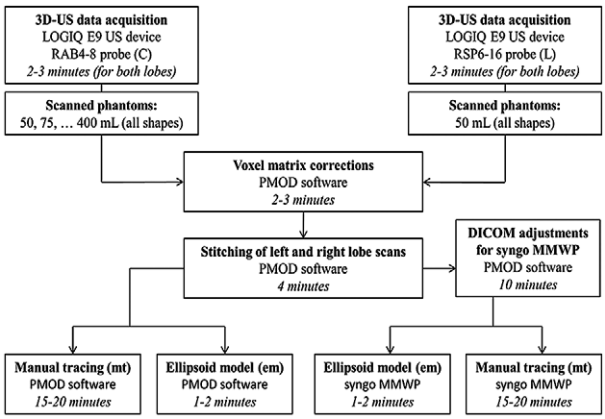

Fig 5. Workflow graph showing the steps from 3D-US data acquisition to final volume measurements. PMOD = research software; syngo MMWP (Multimodality Workplace) = clinical software.

The C-probe data revealed very similar results for cs and rs calculations. However, considerably smaller deviations, higher SDs and wider 95% CI were observed for the em method in comparison to the mt approach. The anatomical variants (nodular shaped and thickened isthmus phantoms) showed markedly higher deviations in comparison to the regular shaped phantoms, especially for the em method. The volumes of regular shaped phantoms were significantly overestimated with both the em and mt methods (em > mt).

Since the L-probe was only applicable for 50 mL phantoms, no reliable data could be acquired. For the 50 mL phantoms an overestimation of approximately 10% was

Table I. Correlation and deviation analyses of convex RAB4-8 probe (C-probe) volume measurements in comparison to the reference volumes.

Method	Phantom shape	Software	Rho*	Percentage deviation				
				Mean±SD	Median	Range	95% CI	Mean ± 1.96*SD (limits of agreement)
Ellipsoid model	regular	cs	0.9982	3.9±4.2	5.9	-4.9 - 7.6	1.6, 6.3	-4.4, 12.2
		rs	0.9982	3.8±4.1	5.6	-5.0 - 7.4	1.6, 6.1	-4.1, 11.8
	nodular	cs	0.9866	2.1±8.7	7.2	-12.8 - 12.5	-2.7, 6.9	-15.0, 19.2
		rs	0.9851	1.8±8.5	6.2	-12.4 - 11.8	-2.9, 6.5	-14.8 , 18.4
	thick isthmus	cs	0.9827	-2.4±9.4	-8.1	-11.0 - 12.9	-7.6, 2.8	-20.8 , 16.1
		rs	0.9843	-2.4±8.8	-7.7	-10.2 - 12.8	-7.3, 2.5	-19.8 , 14.9
Manual tracing	regular	cs	0.9992	1.8±2.1	1.8	-2.4 - 5.9	0.6, 3.0	-2.3 , 5.9
		rs	0.9988	3.2±2.2	3.8	-1.6 - 5.9	1.9, 4.4	-1.2 , 7.5
	nodular	cs	0.9986	1.1±3.6	1.2	-5.3 - 6.0	-0.9, 3.1	-5.9 , 8.1
		rs	0.9987	1.6±3.9	2.2	-5.0 - 6.8	-0.5, 3.8	-6.1 , 9.3
	thick isthmus	cs	0.9972	2.2±4.7	1.0	-4.3 - 15.3	-0.5, 4.8	-7.1 , 11.4
		rs	0.9992	2.5±2.5	2.2	-0.8 - 8.5	1.1, 3.9	-2.5 , 7.4

Rho*: correlation coefficient according to Bravais-Pearson analyses; 95% CI: 95% confidence interval of the mean; cs: clinical software (syngo Multimodality Workplace); rs: research software (PMOD).

observed with the em method (for all phantom shapes) while mt method showed smaller deviations (<5%).

All individual volume measurement data are shown in tabels II-IV.

Table II. Individual volume data of the regular shaped phantoms

Actual phantom volume (mL)	**Volume measurements with different methods and software types (mL)**			
	em, rs	em, cs	mt, rs	mt, cs
48.90	52.52 52.39 (L)	52.54 52.22 (L)	51.74 49.82 (L)	51.77 49.12 (L)
82.14	79.56	79.99	82.15	83.23
95.56	93.61	91.22	98.56	97.45
122.55	123.93	127.11	125.34	124.01
146.00	153.38	152.61	150.94	150.85
169.12	180.49	182.02	175.62	175.83
193.96	204.11	205.53	197.06	193.86
216.08	228.92	229.31	227.63	219.89
238.23	226.20	226.67	234.39	232.50
266.45	282.59	282.73	278.13	278.63
294.09	314.40	311.52	307.57	296.30
317.79	335.63	332.27	330.91	325.21
344.88	366.79	366.54	359.44	352.62
366.34	389.06	389.96	388.07	363.43
391.20	411.98	414.12	392.93	394.65

Em: ellipsoid model; rs: research software (PMOD); cs: clinical software (syngo Multimodality Workplace); mt: manual tracing; L: linear RSP6-16 probe (all other values are acquired with the convex RAB4-8 probe).

Table III. Individual volume data of the nodular shaped phantoms

Actual phantom volume (mL)	**Volume measurements with different methods and software types (mL)**			
	em, rs	em, cs	mt, rs	mt, cs
48.90	53.08 53.08 (L)	53.75 54.01 (L)	46.76 50.29 (L)	46.65 49.76 (L)
82.14	87.22	88.28	83.26	81.30
95.56	83.74	83.31	90.82	93.03
122.55	132.54	131.35	119.77	124.63
146.00	158.32	158.76	152.06	154.46
169.12	155.40	154.54	162.16	160.21
193.96	183.18	181.00	194.65	191.93
216.08	202.27	202.59	228.5	228.54
238.23	221.51	219.64	247.86	241.03
266.45	292.44	293.58	276.23	282.45
294.09	318.77	319.23	300.67	300.79
317.79	355.44	357.44	339.5	332.47
344.88	370.14	369.76	366.86	348.88
366.34	388.83	392.51	378.07	370.78
391.20	359.58	370.44	399.72	396.99

Em: ellipsoid model; rs: research software (PMOD); cs: clinical software (syngo Multimodality Workplace); mt: manual tracing; L: linear RSP6-16 probe (all other values are acquired with the convex RAB4-8 probe).

Table IV. Individual volume data of the thickened isthmus shaped phantoms

Actual phantom volume (mL)	Volume measurements with different methods and software types (mL)			
	em, rs	em, cs	mt, rs	mt, cs
48.90	53.89 52.81 (L)	55.22 53.33 (L)	47.05 49.66 (L)	48.49 48.27 (L)
82.14	74.73	73.72	81.85	81.52
95.56	88.22	87.70	95.66	93.89
122.55	111.64	112.56	124.66	127.49
146.00	164.67	163.49	158.34	168.30
169.12	155.07	155.45	171.06	177.58
193.96	174.18	172.64	198.31	198.15
216.08	198.43	198.33	226.47	218.18
238.23	215.89	212.57	249.3	251.98
266.45	289.12	289.99	275.08	279.70
294.09	273.33	273.16	291.84	281.49
317.79	296.24	295.40	325.6	320.93
344.88	316.02	316.17	357.61	354.20
366.34	398.96	402.48	382.01	370.17
391.20	418.95	422.37	399.98	390.91

Em: ellipsoid model; rs: research software (PMOD); cs: clinical software (syngo Multimodality Workplace); mt: manual tracing; L: linear RSP6-16 probe (all other values are acquired with the convex RAB4-8 probe).

Discussions

Volumetric analyses of thyroid glands are routinely performed in 2D-US technique. However, several 3D-US approaches have been introduced in phantom and human studies showing highly correlative results for volumetric analyses compared with 2D-US [12,17,19,26-28]. The possibility of post hoc evaluations in three different dimensions likewise CT or MRI is favorable in 3D-US. Furthermore, inter-observer assessments showed less variable results in this regard [13-15,29]. However, a remarkable limitation of 3D-US in comparison to clinically established sectional imaging applications such as CT and MRI is the relatively limited FOV. This restricts the interpretation of anatomical contexts and particularly limits the measurement of large thyroid volumes. Therefore, several EFOV approaches have been investigated [21,30-33]. One strategy, stitching of two or more separately acquired 3D-US datasets, has been published in different fields, e.g. cardiology, anesthesiology, and orthopedics [34-37]. The first study assessing volumetric analyses of 3D-US EFOV images of thyroid phantoms has been recently introduced [22]. The results show that stitching of separately obtained 3D-US datasets of differently sized and shaped, elaborately constructed phantoms up to 400 mL acquired via sn US probes was possible and volumetric analyses results were even more accurate than other phantom studies without application of the stitching technique [12]. Both em and mt methods indicated that 3D-US EFOV may be promising for thyroid volumetric analyses.

There are some advantages of ms US probes over the previously published data for sn approaches. Firstly, ms 3D-US is more widely established in clinical fields, especially in prenatal diagnostics [23]. A fourth dimension, continuous temporal resolution, can be applied allowing the assessment of fetal movements [38]. Secondly, the magnetic field necessary for sn investigations, is redundant with ms probes. Consequently, no disturbances of the magnetic field generated by an external magnet can occur and the additional sensor-clips attached to the US probes are unnecessary. Thirdly, the ms probes investigated in the present study automatically generate a 3D volume dataset by means of an incorporated motorized array. The US probe position is fixed throughout the entire image acquisition and therefore the examinations are less operator-dependent than sn data. Nevertheless, patient and operator movements can affect the accuracy even for mt US probes. A possible solution approach to decrease the operator-dependency might be the detachment of the US probe to a steady holding arm.

The investigated L-probe was only suitable for 50 mL phantoms. Due to the absence of virtual convex imaging, the FOV was bilaterally restricted. Therefore, no

data for phantoms >50 mL could be obtained. For the 50 mL phantoms (all shapes), an overestimation of approximately 10% was observed with the em method, while the mt method accurately determined the actual volumes.

The C-probe was successfully applied to all phantoms, regardless of size or shape. The full extent of all phantoms could be captured with one scan per lobe, even for the 400 mL phantoms. In accordance to the previously published sn data, very high correlation coefficients of measured and reference volumes could be achieved [22].

In general, the em method showed markedly higher deviations than the mt method, especially for the non-regular shaped phantoms. In nodular or thickened isthmus shaped phantoms the measurement failures ubiquitously ranged between >-10% and >+10% which may lead to relevant miscalculations, e.g. in the case of activity determinations in preparation of radioiodine therapies. Similar results have already been observed with sn US probes [22]. Taking into account that volume enlargements of the human thyroid gland are frequently associated with deformations of the natural anatomy, the em method should be critically scrutinized in these cases and additional mt volumetric analyses should be considered. However, since the mt method is based on manually drawn ROIs, which are highly subjective and dependent on the user experience, it can hardly be used as a reference standard for statistical evaluations. The current study confirms this limitation by the fact that deviations of up to 15% have been observed.

In clinical practice, mt measurements of large thyroid volumes are usually calculated on the basis of CT images, which is associated with additional radiation exposure [39]. 3D-US EFOV acquired with ms US probes proved to be an accurate alternative without contraindications or side effects. In accordance to the sn data, the mt volumetric analyses of the ms US probes revealed deviations < 10% (exclusive the above mentioned outlier) even for non-regular shaped and large thyroid phantoms.

Nevertheless, the time expenditure for ms 3D-US EFOV volumetric analyses is remarkable. The full workflow for the mt method took 33-40 minutes (em: 19-22 minutes). In contrast, the sn data were obtained within 23-31 minutes (em: 7-13 minutes). The increased time required for ms data is caused by the need for several data modifications. Therefore, an implementation into the clinical practice is widely restricted in its current form. For this purpose, improvements with regard to the data processing need to be carried out by the manufacturers. Several approaches addressing automated segmentation by tissue echogenicity differences have been introduced, e.g. left atrial volumes in 3D echocardiography [40]. Furthermore, the clinical relevance of the stitching technique is yet to be determined, and clinical studies are warranted. It remains unclear if appropriate anatomical landmarks, which are necessary for the creation of a stitched EFOV dataset, can be determined in human subjects. In previous clinical studies investigating fusion imaging in human thyroid glands, the trachea, the hyoid bone, cervical vertebral bodies, and calcified nodules (if applicable), were described as suitable landmarks for the alignment of CT and US images [41]. These constant anatomical structures might be suitable landmarks for the presented stitching method as well.

Conclusions

3D-US EFOV stitching of two separate 3D-US datasets proved feasible and accurate for the investigated mechanically-swept convex RAB4-8 US probe. Precise volumetric analyses of even large thyroid phantoms (up to 400 mL) have been carried out. The results of the manual tracing method were superior (but more time consuming) compared to the ellipsoid model approach. The very high correlation coefficients between measured and reference volumes were similar to previously investigated sensor-navigated US probes. Further improvements regarding the data processing need to be achieved in order to reduce the time expenditure and make the approach suitable for the implementation into clinical fields. We did not observe relevant differences between the investigated clinical or research software types. The investigated mechanically-swept linear RSP6-16 probe was restricted to 50 mL phantoms and therefore appears to be inappropriate for the examination of large volume subjects.

Conflict of interest: none.

Acknowledgements: The authors appreciatively acknowledge the assistance of Hiltrud Niggemann for the statistical analyses. GE Healthcare, Milwaukee, WI, USA is gratefully acknowledged for providing the hardware (LOGIQ E9) for this study.

References

1. Carle A, Krejbjerg A, Laurberg P. Epidemiology of nodular goitre. Influence of iodine intake. Best Pract Res Clin Endocrinol Metab 2014;28:465-479.
2. Duarte GC, Araujo LMQ, Magalhaes F Filho, Almada CM Filho, Cendoroglo MS. Ultrasonographic assessment of thyroid volume in oldest-old individuals. Arch Endocrinol Metab 2017;61:269-275.
3. Duarte GC, Tomimori EK, de Camargo RY, et al. Excessive iodine intake and ultrasonographic thyroid abnormalities in schoolchildren. J Pediatr Endocrinol Metab 2009;22:327-334.

4. Dauksiene D, Petkeviciene J, Klumbiene J, V et al. Factors Associated with the Prevalence of Thyroid Nodules and Goiter in Middle-Aged Euthyroid Subjects. Int J Endocrinol 2017;2017:8401518.
5. Turcios S, Lence-Anta JJ, Santana JL, et al. Thyroid volume and its relation to anthropometric measures in a healthy cuban population. Eur Thyroid J 2015;4:55-61.
6. Haugen BR, Alexander EK, Bible KC, et al. 2015 American Thyroid Association Management Guidelines for Adult Patients with Thyroid Nodules and Differentiated Thyroid Cancer: The American Thyroid Association Guidelines Task Force on Thyroid Nodules and Differentiated Thyroid Cancer. Thyroid 2016;26:1-133.
7. Perros P, Boelaert K, Colley S, et al. Guidelines for the management of thyroid cancer. Clin Endocrinol (Oxf) 2014;81 Suppl 1:1-122.
8. Dighe M, Barr R, Bojunga J, et al. Thyroid Ultrasound: State of the Art Part 1 - Thyroid Ultrasound reporting and Diffuse Thyroid Diseases. Med Ultrason 2017;19:79-93.
9. Salvatori M, Luster M. Radioiodine therapy dosimetry in benign thyroid disease and differentiated thyroid carcinoma. Eur J Nucl Med Mol Imaging 2010;37:821-828.
10. Park SB, Kang BS. Value of ultrasonographic evaluation for soft-tissue lesions: focus on incidentally detected lesions on CT/MRI. Jpn J Radiol 2017;35:485-494.
11. Suzuki S, Midorikawa S, Fukushima T, et al. Systematic determination of thyroid volume by ultrasound examination from infancy to adolescence in Japan: the Fukushima Health Management Survey. Endocr J 2015;62:261-268.
12. Freesmeyer M, Wiegand S, Schierz JH, Winkens T, Licht K. Multimodal evaluation of 2-D and 3-D ultrasound, computed tomography and magnetic resonance imaging in measurements of the thyroid volume using universally applicable cross-sectional imaging software: a phantom study. Ultrasound Med Biol 2014;40:1453-1462.
13. Andermann P, Schlogl S, Mader U, Luster M, Lassmann M, Reiners C. Intra- and interobserver variability of thyroid volume measurements in healthy adults by 2D versus 3D ultrasound. Nuklearmedizin 2007;46:1-7.
14. Schlogl S, Andermann P, Luster M, Reiners C, Lassmann M. A novel thyroid phantom for ultrasound volumetry: determination of intraobserver and interobserver variability. Thyroid 2006;16:41-46.
15. Vulpoi C, Mogos V, Ciobanu DG, et al. Thyroid ultrasonography. Interobserver and intraobserver variations. Rev Med Chir Soc Med Nat Iasi 2007;111:864-871.
16. Freesmeyer M, Darr A, Schierz JH, Schleussner E, Wiegand S, Opfermann T. 3D ultrasound DICOM data of the thyroid gland. First experiences in exporting, archiving, second reading and 3D processing. Nuklearmedizin 2012;51:73-78.
17. Schlogl S, Werner E, Lassmann M, et al. The use of three-dimensional ultrasound for thyroid volumetry. Thyroid 2001;11:569-574.
18. Shu JA, Zhao JN, Guo DJ, Luo YD, Zhong WJ, Xie WB. Accuracy and reliability of thyroid volumetry using spiral CT and thyroid volume in a healthy, non-iodine-deficient Chinese adult population. Eur J Radiol 2011;77:274-280.
19. Lyshchik A, Drozd V, Reiners C. Accuracy of three-dimensional ultrasound for thyroid volume measurement in children and adolescents. Thyroid 2004;14:113-120.
20. Shapiro RS. Panoramic ultrasound of the thyroid. Thyroid 2003;13:177-181.
21. Ma YL, Rhode KS, Gao G, et al. Ultrasound calibration using intensity-based image registration: for application in cardiac catheterization procedures. Proc SPIE 2008;6918:69180O. doi: 10.1117/12.770174.
22. Freesmeyer M, Knichel L, Kuehnel C, Winkens T. Stitching of sensor-navigated 3D ultrasound datasets for the determination of large thyroid volumes - a phantom study. Med Ultrason 2018;20:480-486.
23. Merz E. 25 Years of 3D ultrasound in prenatal diagnosis (1989-2014). Ultraschall Med 2015;36:3-8.
24. Bland JM, Altman DG. Statistical methods for assessing agreement between two methods of clinical measurement. Lancet 1986;1:307-310.
25. Giavarina D. Understanding Bland Altman analysis. Biochem Med (Zagreb) 2015;25:141-151.
26. Ng E, Chen T, Lam R, Sin D, Ying M. Three-dimensional ultrasound measurement of thyroid volume in asymptomatic male Chinese. Ultrasound Med Biol 2004;30:1427-1433.
27. Rago T, Bencivelli W, Scutari M, et al. The newly developed three-dimensional (3D) and two-dimensional (2D) thyroid ultrasound are strongly correlated, but 2D overestimates thyroid volume in the presence of nodules. J Endocrinol Invest 2006;29:423-426.
28. Malago R, D'Onofrio M, Ferdeghini M, et al. Thyroid volumetric quantification: comparative evaluation between conventional and volumetric ultrasonography. J Ultrasound Med 2008;27:1727-1733.
29. Tong S, Cardinal HN, McLoughlin RF, Downey DB, Fenster A. Intra- and inter-observer variability and reliability of prostate volume measurement via two-dimensional and three-dimensional ultrasound imaging. Ultrasound Med Biol 1998;24:673-681.
30. Poon TC, Rohling RN. Three-dimensional extended field-of-view ultrasound. Ultrasound Med Biol 2006;32:357-369.
31. Dyer E, Zeeshan Ijaz U, Housden R, Prager R, Gee A, Treece G. A clinical system for three-dimensional extended-field-of-view ultrasound. Br J Radiol 2012;85:e919-e924.
32. Wachinger C, Wein W, Navab N. Three-dimensional ultrasound mosaicing. Med Image Comput Comput Assist Interv 2007;10:327-335.
33. Ying M, Sin MH. Comparison of extended field of view and dual image ultrasound techniques: accuracy and reliability of distance measurements in phantom study. Ultrasound Med Biol 2005;31:79-83.
34. Reiter M, Ulreich N, Dirisamer A, Tscholakoff D, Bucek RA. [Extended field-of-view sonography in Achilles tendon disease: a comparison with MR imaging]. Rofo. 2004;176:704-708.
35. Brekke S, Rabben SI, Stoylen A, et al. Volume stitching in three-dimensional echocardiography: distortion analysis and extension to real time. Ultrasound Med Biol 2007;33:782-796.

36. Hayworth KJ, Xu CS, Lu Z, et al. Ultrastructurally smooth thick partitioning and volume stitching for large-scale connectomics. Nat Methods 2015;12:319-322.
37. Schneider RJ, Perrin DP, Vasilyev NV, Marx GR, Del Nido PJ, Howe RD. Real-time image-based rigid registration of three-dimensional ultrasound. Med Image Anal 2012;16:402-414.
38. Sajapala S, AboEllail MAM, Kanenishi K, Mori N, Marumo G, Hata T. 4D ultrasound study of fetal movement early in the second trimester of pregnancy. J Perinat Med 2017;45:737-743.
39. Lee SJ, Chong S, Kang KH, et al. Semiautomated thyroid volumetry using 3D CT: prospective comparison with measurements obtained using 2D ultrasound, 2D CT, and water displacement method of specimen. AJR Am J Roentgenol 2014;203:W525-W532.
40. Almeida N, Papachristidis A, Pearson P, S et al. Left atrial volumetric assessment using a novel automated framework for 3D echocardiography: a multi-centre analysis. Eur Heart J Cardiovasc Imaging 2017;18:1008-1015.
41. Seifert P, Winkens T, Kuhnel C, Guhne F, Freesmeyer M. I-124-PET/US Fusion Imaging in Comparison to Conventional Diagnostics and Tc-99m Pertechnetate SPECT/US Fusion Imaging for the Function Assessment of Thyroid Nodules. Ultrasound Med Biol. 2019 Jun 10. doi: 10.1016/j.ultrasmedbio.2019.05.008.